

## ONE MOMENT IN TIME - MODELING STAR FORMATION IN THE ANTENNAE

SIMON J. KARL<sup>1</sup>, THORSTEN NAAB<sup>1,2</sup>, PETER H. JOHANSSON<sup>1</sup>, HANNA KOTARBA<sup>1</sup>, CHRISTIAN M. BOILY<sup>3</sup>, FLORENT RENAUD<sup>3,4</sup>, CHRISTIAN THEIS<sup>4,5</sup>

<sup>1</sup> Universitäts-Sternwarte München, Scheinerstr. 1, D-81679 München, Germany;  
skar1@usm.lmu.de

<sup>2</sup> Max-Planck-Institut für Astrophysik, Karl-Schwarzschild-Str. 1, D-85741 Garching bei München, Germany;  
naab@mpa-garching.mpg.de

<sup>3</sup> Observatoire astronomique, Université de Strasbourg and CNRS UMR 7550,  
11 rue de l'Université, F-67000 Strasbourg, France

<sup>4</sup>Institut für Astronomie der Univ. Wien, Türkenschanzstr. 17, A-1180 Vienna, Austria and

<sup>5</sup> Planetarium Mannheim, Wilhelm-Varnholt-Allee 1, D-68165 Mannheim, Germany

Accepted for publication in *ApJL*.

### ABSTRACT

We present a new high-resolution N-body/SPH simulation of an encounter of two gas-rich disk galaxies which closely matches the morphology and kinematics of the interacting Antennae galaxies (NGC 4038/39). The simulation includes radiative cooling, star formation and feedback from SNI. The large-scale morphology and kinematics are determined by the internal structure and the orbit of the progenitor disks. The properties of the central region, in particular the starburst in the overlap region, only match the observations for a very short time interval ( $\Delta t \approx 20$  Myr) after the second encounter. This indicates that the Antennae galaxies are in a special phase only about 40 Myr after the second encounter and 50 Myr before their final collision. This is the only phase in the simulation when a gas-rich overlap region between the nuclei is forming accompanied by enhanced star formation. The star formation rate as well as the recent star formation history in the central region agree well with observational estimates. For the first time this new model explains the distributed extra-nuclear star formation in the Antennae galaxies as a consequence of the recent second encounter. The proposed model predicts that the Antennae are in a later merger stage than the Mice (NGC 4676) and would therefore lose their first place in the classical Toomre sequence.

*Subject headings:* galaxies: evolution — galaxies: individual (NGC 4038/39) — galaxies: interactions — galaxies: star formation — methods: numerical

### 1. INTRODUCTION

In the local universe ( $z < 0.3$ ) about  $\sim 5 - 10\%$  of all galaxies are interacting and merging (e.g. Lotz et al. 2008; Bridge et al. 2010). Mass assembly via this mechanism was more important at earlier cosmic times when major mergers were more frequent (e.g. Patton et al. 2002; Conselice et al. 2003) and also more gas-rich (e.g. Tacconi et al. 2010). Major mergers dramatically affect the formation and evolution of galaxies. By inducing tidal torques they can efficiently transport gas to the centers of the galaxies (Barnes & Hernquist 1996; Naab et al. 2006), trigger star formation (Mihos & Hernquist 1996; Springel 2000; Cox et al. 2008), feed super-massive black holes (Hopkins et al. 2005; Springel et al. 2005; Johansson et al. 2009) and convert spiral galaxies into intermediate-mass ellipticals (Barnes 1992; Naab & Burkert 2003; Rothberg & Joseph 2004; Naab & Ostriker 2009).

The Antennae galaxies (NGC 4038/39) are the nearest and best-studied example of an on-going major merger of two gas-rich spiral galaxies. The system sports a beautiful pair of elongated tidal tails extending to a projected size of  $\sim 20'$  (i.e. 106 kpc at an assumed distance of 22 Mpc), together with two clearly visible, still distinct galactic disks. The latter has been assumed to be an indication of an early merger state, putting the system in the first place of the Toomre (1977) merger sequence of 11 prototypical mergers. Due to their proximity and the ample number of high-quality observa-

tions covering the spectrum from radio to X-ray (e.g. Neff & Ulvestad 2000; Wang et al. 2004; Whitmore et al. 1999; Hibbard et al. 2005; Zezas et al. 2006) the Antennae provide an ideal laboratory for understanding the physics of merger-induced starbursts through comparison with high-resolution simulations.

At the center of the Antennae galaxies, HST imaging has revealed a large number of bright young star clusters ( $\gtrsim 1000$ ) which plausibly have formed in several bursts of star formation induced by the interaction (Whitmore et al. 1999). The spatial distribution and the age of these clusters are correlated: the youngest clusters are found in the overlap region ( $\tau < 5$  Myr), while the young starburst is generally located in the overlap and a ring-like configuration in the disk of NGC 4038 ( $\tau \lesssim 30$  Myr). An intermediate-age population ( $\tau = 500 - 600$  Myr) is distributed throughout the disk of NGC 4038 (Whitmore et al. 1999; Zhang et al. 2001).

Of particular interest is the spectacular nature of an extra-nuclear starburst observed in the dusty overlap region between the merging galactic disks (Mirabel et al. 1998; Wang et al. 2004). The Antennae seem to be the only interacting system where an off-center starburst is outshining the galactic nuclei in the mid-IR (Xu et al. 2000) and among only a few systems which show enhanced inter-nuclear gas concentrations (Tacconi et al. 1999). To date, this prominent feature has not been reproduced in any simulation of the Antennae system (see Barnes & Hibbard 2009). Thus, the question remains whether this feature cannot be captured by current sub-

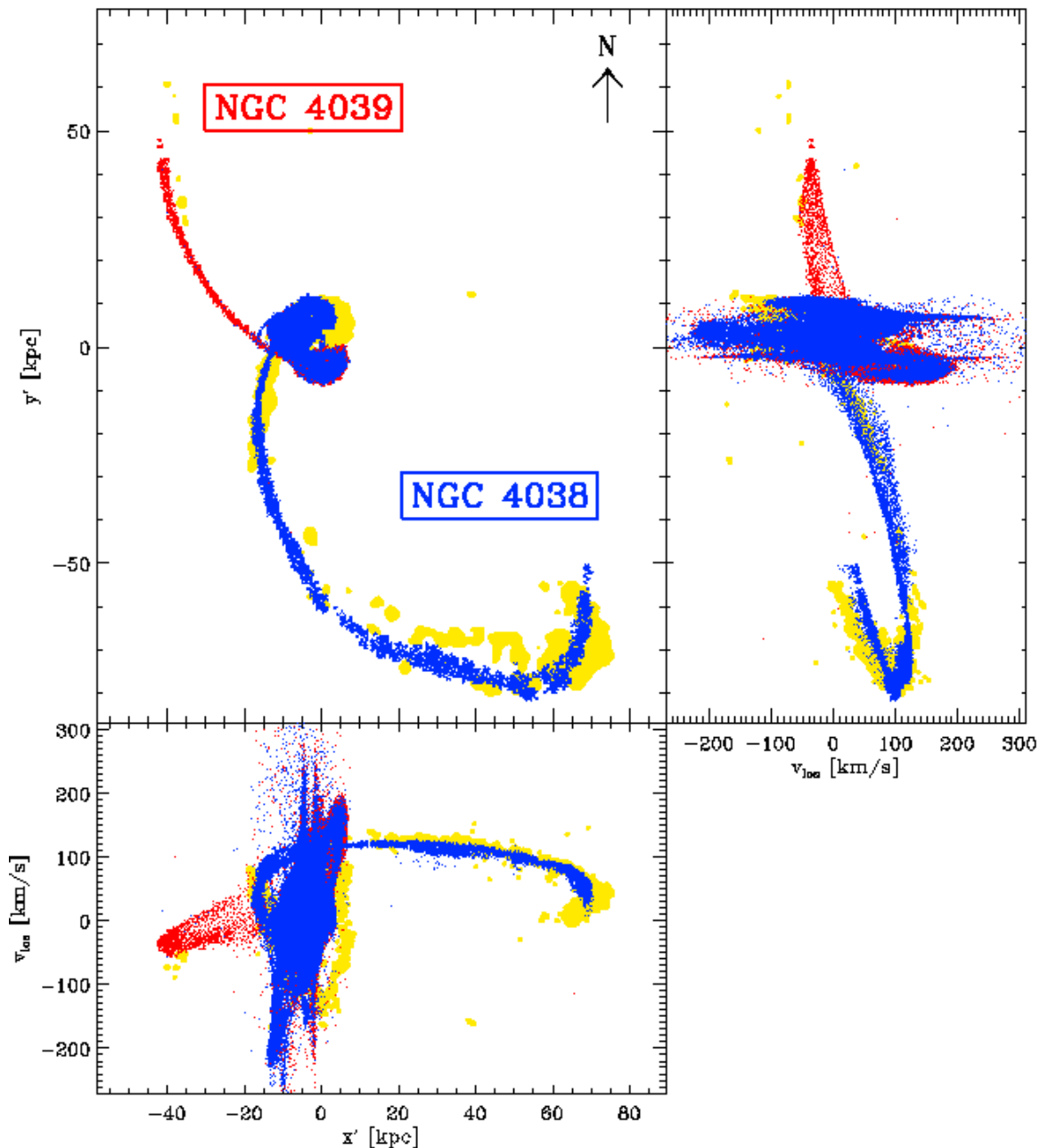


FIG. 1.— Simulated gas properties projected on top of HI kinematic data by Hibbard et al. (2001) at the time of best match. Simulated gas particles are displayed in blue (NGC 4038) and red (NGC 4039). Yellow points represent the observational data. *Upper left panel:* Projected positions in the plane-of-the-sky ( $x'$ - $y'$  plane). *Upper right and lower left panel:* Declination ( $y'$ ) and Right Ascension ( $x'$ ) against line-of-sight velocity. Similarly to the observations, we apply a column density threshold of  $N_{\text{gas}} = 10^{20} \text{ cm}^{-2}$  to the simulated gas distribution.

grid modeling of star formation or whether the previous dynamical models (e.g. initial conditions) were not accurate enough.

A first simulation of the Antennae galaxies was presented by Toomre & Toomre (1972), reproducing the correct trends in the morphology of the tidal tails. Barnes (1988) repeated the analysis with a self-consistent multi-component model consisting of a bulge, disk and dark halo component. Mihos et al. (1993) included gas and star formation in their model and found the star formation to be concentrated in the nuclei of the disks, thus, not reproducing the overlap star formation.

In this Letter, we present the first high-resolution

merger simulation of NGC 4038/39 with cosmologically motivated progenitor disks galaxy models. We are able to match both the large-scale morphology and the line-of-sight kinematics, as well as important key aspects of the distribution and ages of newly-formed stars at the center of the Antennae, being a direct consequence of the improved merger orbit.

## 2. SIMULATIONS

The simulation presented here is the best-fitting model of a larger parameter study and was performed using GADGET 2 (Springel 2005). We include primordial radiative cooling and a local extra-galactic UV background. Star formation and associated SNII feedback are mod-

TABLE 1  
MODEL PARAMETERS OF THE BEST-FIT MERGER CONFIGURATION

Property	NGC 4038	NGC 4039
$M_{\text{vir}}^a$	55.2	55.2
$M_{\text{disk,stellar}}$	3.3	3.3
$M_{\text{disk,gas}}$	0.8	0.8
$M_{\text{bulge}}$	1.4	1.4
$r_{\text{disk}}^b$	6.28	4.12
$z_0$	1.26	0.82
$r_{\text{bulge}}$	1.26	0.82
$c^c$	15	15
$\lambda^d$	0.10	0.07
$v_{\text{rot}}^{\text{max}e}$	189	198

<sup>a</sup>Mass in  $10^{10} M_{\odot}$

<sup>b</sup>Disk and bulge lengths ( $r_{\text{disk}}$ ,  $r_{\text{bulge}}$ ) and disk scale height ( $z_0$ ) are given in kpc

<sup>c</sup>Halo concentration parameter

<sup>d</sup>Halo spin parameter

<sup>e</sup>Maximum rotational velocity in  $\text{km s}^{-1}$

eled following the sub-grid multi-phase prescription of Springel & Hernquist (2003), but excluding supernovae-driven galactic winds. For densities  $n > n_{\text{crit}} = 0.128 \text{ cm}^{-3}$  the ISM is treated as a two-phase medium with cold clouds embedded in pressure equilibrium in a hot ambient medium. We deploy a fiducial set of parameters governing the multi-phase feedback model resulting in a star formation rate (SFR) of  $\sim 1 M_{\odot} \text{ yr}^{-1}$  for a Milky Way-type galaxy. We adopt a softened equation of state (EQS) with  $q_{\text{EQS}} = 0.5$ , where the parameter  $q_{\text{EQS}}$  interpolates the star formation model between the full feedback model ( $q_{\text{EQS}} = 1.0$ ) and an isothermal EQS with  $T = 10^4 \text{ K}$  ( $q_{\text{EQS}} = 0$ ) (see Springel et al. 2005 for further details). The progenitor galaxies are set up in equilibrium according to the method of Springel et al. (2005) with a total virial mass of  $M_{\text{vir}} = 5.52 \times 10^{11} M_{\odot}$  for each galaxy. The dark matter halos are constructed using a Hernquist (1990) density profile. They are populated with exponential stellar disks comprising a constant disk mass fraction  $m_{\text{d}} = 0.075$  of the total virial mass and a stellar Hernquist bulge with a bulge mass fraction of  $m_{\text{b}} = 0.025$  ( $m_{\text{b}} = 1/3m_{\text{d}}$ ). The gas mass fraction of the disk component is  $f_{\text{g}} = 0.2$  with the rest of the disk mass remaining in stars. The disk and bulge scale lengths are determined using the Mo, Mao, & White (1998) formalism. A summary of the most relevant model parameters is given in Table 1.

Each galaxy is realized with  $N_{\text{tot}} = 1.2 \times 10^6$  particles, i.e. 400,000 halo particles, 200,000 bulge particles, 480,000 disk particles and 120,000 SPH particles. In order to avoid spurious two-body effects we ensured that all baryonic particles have the same mass and only *one* stellar particle is spawned per SPH particle. This yields a total baryon fraction of  $f_{\text{bary}} = 10\%$  with particle masses for the baryonic components (bulge, disk, formed stars, and gas) of  $m_{\text{bary}} = 6.9 \times 10^4 M_{\odot}$  and  $m_{\text{DM}} = 1.2 \times 10^6 M_{\odot}$  for the dark matter particles.

The gravitational softening lengths are set to  $\epsilon_{\text{bary}} = 0.035 \text{ kpc}$  for baryons, and  $\epsilon_{\text{DM}} = 0.15 \text{ kpc}$  for dark matter particles, scaled according to  $\epsilon_{\text{DM}} = \epsilon_{\text{bary}} (m_{\text{DM}}/m_{\text{bary}})^{1/2}$ .

We adopt an initially nearly-parabolic, prograde orbit geometry (the orbital plane lies in the x-y plane) with a pericenter distance of  $r_{\text{p}} = r_{\text{d,4038}} + r_{\text{d,4039}} = 10.4 \text{ kpc}$

and an initial separation of  $r_{\text{sep}} = r_{\text{vir}} = 168 \text{ kpc}$ . For the orientation of the progenitor disks we found the best match to the Antennae system with inclinations  $i_{4038} = 60^\circ$ ,  $i_{4039} = 60^\circ$  and arguments of pericenter  $\omega_{4038} = 30^\circ$ ,  $\omega_{4039} = 60^\circ$  (see Toomre & Toomre 1972).

### 3. RESULTS

#### 3.1. The morphological and kinematical match

We determine the time when the simulation best matches the Antennae together with the viewing angles ( $\theta, \psi, \phi$ ) which specify a series of subsequent rotations around the x-, y-, and z-axis. In the further analysis we will use the rotated 3D position-velocity subspace, i.e. the plane-of-the-sky (x'-y' plane) and the line-of-sight velocity  $v_{\text{los}}$ , for comparison with the observations. Finally, we apply a distance scale ( $\mathcal{L}$ ) relative to a fiducial distance of 22 Mpc (Schweizer et al. 2008)<sup>1</sup> and assume a systemic helio-centric velocity of  $1630 \text{ km s}^{-1}$  to fit the observational data to the physical scales in the simulation.

We find our best match to the observed large- and small-scale properties of the system with viewing angles of (93, 69, 253.5) and  $\mathcal{L} = 1.4$ , yielding a distance of  $D = 30.8 \text{ Mpc}$  to the system. The "best fit" ( $t = 1.24 \text{ Gyr}$  after beginning of the simulation) is reached only  $\sim 40 \text{ Myr}$  after the second encounter ( $t = 1.20 \text{ Gyr}$ ), and approximately 50 Myr before the final merging of the galaxy centers ( $t = 1.29 \text{ Gyr}$ ). From our larger parameter study we found this exact timing to be a mandatory requirement for reproducing the overlap starburst. The first close passage of the two progenitor disk galaxies occurred  $\sim 600 \text{ Myr}$  ago which is considerably longer ago than  $\sim 200 - 400 \text{ Myr}$  as suggested in earlier models (Barnes 1988; Mihos et al. 1993) and in much better agreement with observed 'intermediate-age' star clusters ( $\sim 500 - 600 \text{ Myr}$ ). In Fig.1 we show three large-scale projections of the PV cube of our simulated gas particles (NGC 4038: blue, NGC 4039: red) together with a direct comparison to HI observations (yellow) by Hibbard et al. (2001). The HI gas phase is used here as a tracer for the smooth underlying morphological and kinematical structure of the gas in the Antennae and we apply, similarly to the HI observations a column density threshold of  $N_{\text{HI}} \leq 1 \times 10^{20} \text{ cm}^{-2}$  in the simulation. The top left panel displays the plane-of-the-sky projection, while in the top right and bottom left panels we show two orthogonal position-velocity profiles, Declination versus  $v_{\text{los}}$  (upper right) and  $v_{\text{los}}$  versus Right Ascension (lower left). The simulation matches the morphology and kinematics of the observed system very closely, especially for the southern arm, including the prominent kink in the velocities at the tip of the tidal arm (see Fig.1, upper right and lower left panels). Due to the different initial orientations of the progenitor disks, the gas distribution in the northern arm is more diffuse than in the southern arm. The assumed column density cut-off therefore

<sup>1</sup> Note that the distance to the Antennae is a matter of recent debate. The systemic recession velocity yields a distance of 19.2 Mpc (assuming  $H_0 = 75 \text{ km s}^{-1} \text{ Mpc}^{-1}$ ) while photometry of the tip of the red giant branch suggests a much shorter distance of only 13.3 Mpc (Saviane et al. 2008). Recently, Schweizer et al. (2008) have used three independent methods to determine a distance of  $22 \pm 3 \text{ Mpc}$ .

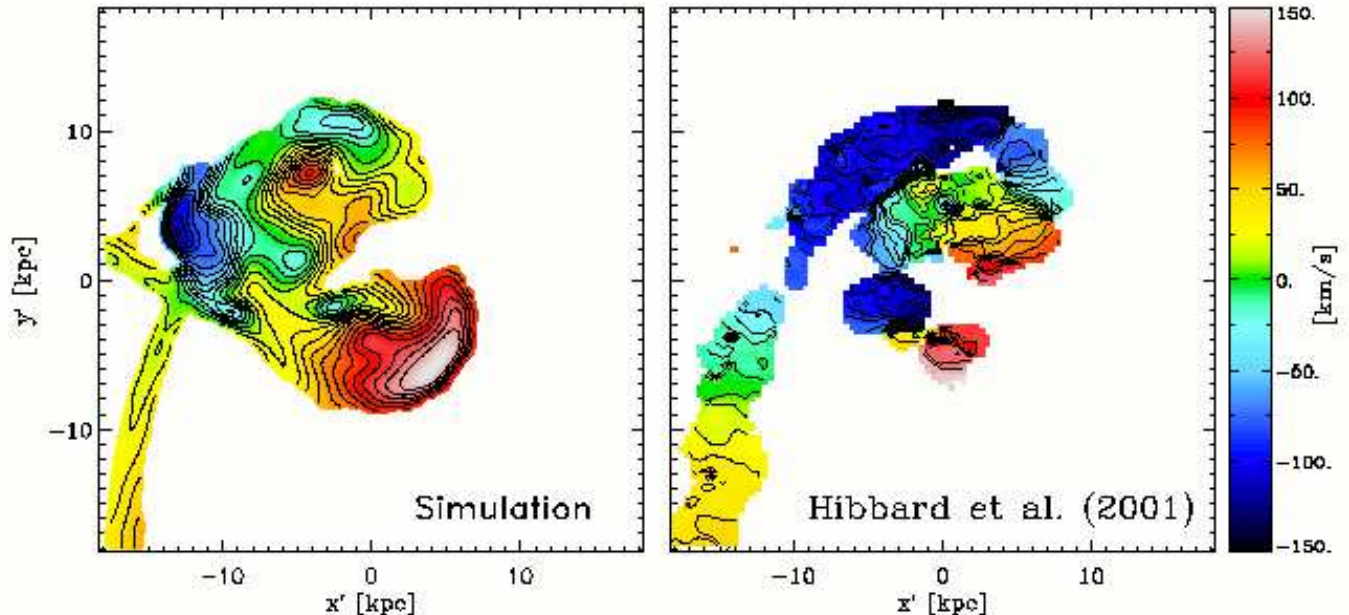


FIG. 2.— Line-of-sight velocity fields inside 18 kpc of the simulated and observed central disks. Isovelocity contours are drawn at  $10 \text{ km s}^{-1}$  intervals ranging from  $-150 \text{ km s}^{-1}$  to  $150 \text{ km s}^{-1}$ . *Left*: density-weighted velocity map. *Right*: intensity-weighted HI velocity field of the high-resolution data cube. A column density threshold is applied as in Fig.1.

results in a similar characteristic stubby geometry as observed (Fig.1, upper left).

A closeup of the simulated and observed line-of-sight gas velocity fields in the central 18 kpc of NGC 4038/39 is shown in the left and right panels of Fig.2. Gas particles are binned on a SPH-kernel weighted  $256^3$  grid and summed up along the line-of-sight to produce a density-weighted velocity map (see Hibbard et al. 2001). The grid is smoothed with the observed beam profile and displayed using the same projected pixel sizes ( $\Delta_{\text{RA}} = 2.64''$  and  $\Delta_{\text{Decl}} = 2.5''$ ) as in Hibbard et al. (2001). We overlay isovelocity contours spaced by  $10 \text{ km s}^{-1}$  and apply the same column density threshold as in Fig.1. The simulation agrees well with the observed velocity field of the disk of NGC 4038. The northern part is approaching and the southern part is receding at similar velocities. Similarly, the simulated disk of NGC 4039 is approaching in the northern part and receding in the southern part like in the observations. In the simulation we have significantly more gas in the overlap region and the southern disk than in the observed HI velocity field. This is due to the fact that we do not distinguish between molecular and atomic gas in our simulation whereas most of the gas in the central regions of the Antennae seems to be in molecular form (Gao et al. 2001).

### 3.2. The recent starburst

In Fig.3 we show a color-coded map of the total gas surface density in the central 18 kpc of the simulation (upper panel). The nuclei of the progenitor disks are still distinct and connected by a bridge of high density gas. In the lower panel of Fig.3 we show the corresponding isodensity contours and overplot in color all stellar particles (with individual masses of  $m_{\text{star}} = 6.9 \times 10^4 M_{\odot}$ ) formed in the last  $\tau < 15 \text{ Myr}$  (blue),  $15 \text{ Myr} < \tau < 50 \text{ Myr}$  (green), and  $50 \text{ Myr} < \tau < 100 \text{ Myr}$  (red). In regions of currently high gas densities the very young stars (blue)

form predominantly at the centers, in the overlap region, as well as in the spiral features around the disks similar to the observed system (Whitmore et al. 1999; Wang et al. 2004), save the fact that the star formation in the centers seems to be much more pronounced in our simulation (see below). However, the overlap region is almost devoid of stars older than 50 Myr (red) indicating that the overlap starburst is a very recent phenomenon. Simulating the system further in time we find that the total duration of the off-center starburst is no longer than  $\approx 20 \text{ Myr}$ .

Brandl et al. (2009) derived SFRs in the nuclei of NGC 4038 ( $0.63 M_{\odot} \text{ yr}^{-1}$ ) and NGC 4039 ( $0.33 M_{\odot} \text{ yr}^{-1}$ ), and a total SFR of  $5.4 M_{\odot} \text{ yr}^{-1}$  for 5 infrared peaks in the overlap region. Comparing these values to simulated SFRs of  $2.9 M_{\odot} \text{ yr}^{-1}$  (NGC 4038) and  $2.8 M_{\odot} \text{ yr}^{-1}$  (NGC 4039) in the galactic nuclei (defined as the central kpc), together with  $1.0 M_{\odot} \text{ yr}^{-1}$  in the overlap region, we find that our simulation still falls short of producing the most intense starburst in the overlap compared to only modest star formation in the nuclei. We note, however, that we find a ratio ( $\text{SFR}_{\text{overlap}}/\text{SFR}_{\text{nuclei}}$ ) of a factor of  $\sim 60$  (!) higher than reported in a previous Antennae model (Mihos et al. 1993). The total SFR of  $8.1 M_{\odot} \text{ yr}^{-1}$  measured from the SPH particles is in good agreement with the range of observed values between  $5 - 20 M_{\odot} \text{ yr}^{-1}$  (e.g. Zhang et al. 2001).

In Fig.4 we plot the formation rate of stellar particles within 18 kpc against their age (solid line). We find a significant increase of the SFR after the first and in particular after the second pericenter (dotted and dashed horizontal lines). Assuming the simulated SFR to be directly proportional to the cluster formation rate we compare the simulated SFR to observations of the age distribution of young star clusters (Fall et al. 2005; Whitmore et al. 2007), using the same time binning of 0.5 dex in  $\log(\tau[\text{yr}])$ . We find that our simulated data are in very good agreement exhibiting a similarly good

match to the observed cluster formation rate as found by Bastian et al. (2009) who compared to the Mihos et al. (1993) Antennae model. This model predicted a nearly constant formation rate for ages  $\tau < 100$  Myr. However, in contrast to the Mihos et al. (1993) model, we find an additional significant increase in the formation rate of young stellar populations at ages  $\tau \lesssim 10$  Myr induced by the recent second encounter. Despite the increase, the predicted formation rates of young clusters are still an order of magnitude lower than observed. Further investigations have to show whether this discrepancy originates from still uncertain details of the star formation model or explicit effects of the early disruption and evolution of massive clusters (“infant mortality”, see e.g. Whitmore et al. 2007; Bastian et al. 2009) which were not included in our model.

In this simulation, and other simulations in our parameter study with similar central properties, we only find prominent star formation in the overlap region for a very short period of time after the second encounter, lasting for only  $\sim 20$  Myr. In addition, stellar feedback is required to prevent the rapid consumption of gas by star formation at earlier times. In a comparison run without stellar feedback most of the gas is consumed efficiently after the first pericenter and not enough gas is left over to form the overlap starburst after the second encounter. Thus, a central conclusion of our study is that the strong localized, off-center starbursts observed in the overlap region stems from a short-lived transient phase in the merging process associated with the recent second encounter.

#### 4. DISCUSSION

The new numerical model for the Antennae galaxies presented in this Letter improves on previous models in several key aspects. We find an excellent morphological and kinematical match to the observed large-scale morphology and HI velocity fields (Hibbard et al. 2001). In addition, our model produces a fair morphological and kinematical representation of the observed central region. A strong off-center starburst naturally develops in the simulation - in good qualitative and quantitative agreement with the observed extra-nuclear star-forming sites (e.g. Mirabel et al. 1998; Wang et al. 2004). This is a direct consequence of our improved merger orbit. All previous studies using traditional orbits failed to reproduce the overlap starburst (see e.g. Karl et al. 2008). The exact timing after the second encounter shortly before the final merger ensures that the galaxies are close enough for the efficient tidally-induced formation of the overlap region. The formation of the extra-nuclear starburst is likely to be supported by compressive tidal forces which can dominate the overlap region in Antennae-like galaxy mergers during close encounters (Renaud et al. 2008, 2009). Energetic feedback from supernovae prevents the depletion of gas by star formation at earlier merger stages and ensures that by the time of the second encounter enough gas is left over to fuel the starburst. Simulating the system with an identical orbit, but now employing an isothermal EQS without feedback from supernovae ( $q_{\text{EQS}} = 0$ ) resulted in most of the gas being depleted by star formation at earlier phases of the merger, i.e. during the first encounter.

Our model predicts that the observed off-center star-

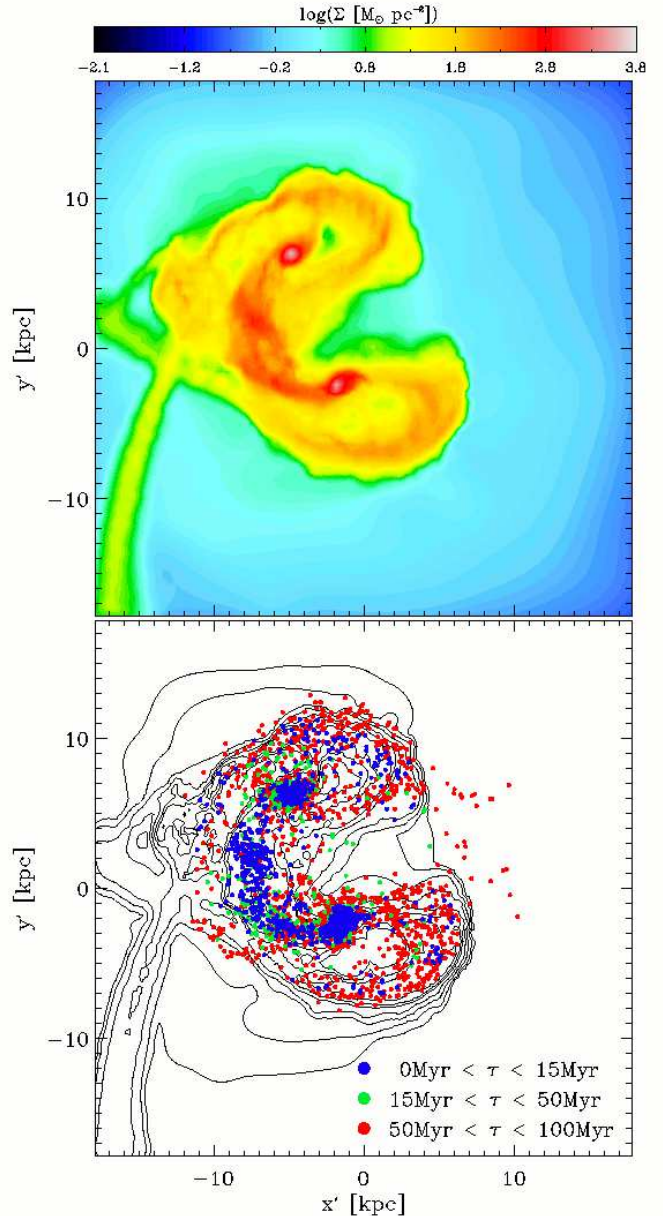


FIG. 3.— *Top*: Gas surface density in the central 18 kpc of the simulation. There are clear concentrations of gas in at the two centers of the galaxies and the overlap region (red contours). *Bottom*: Recently formed stellar particles color-coded by their ages. The youngest stars (blue:  $\tau < 15$  Myr) have formed predominantly in the overlap region and the centers associated with the peaks in the gas surface density, and tidal features around the disks (see upper panel). Older stars (green:  $15 \text{ Myr} < \tau < 50$  Myr; red:  $50 \text{ Myr} < \tau < 100$  Myr) have formed throughout the galactic disks and the tidal arcs.

burst is a transient feature with a very short lifetime ( $\approx 20$  Myr) compared to the full merger process ( $\approx 650$  Myr from first encounter to final merger). This fact serves as a plausible explanation for why such features are rarely observed in interacting galaxies (Xu et al. 2000). However, the observed puzzling gas concentration between the two nuclei of the NGC 6240 merger system might be of a similar origin (Tacconi et al. 1999, Engel in prep. 2010) suggesting that the Antennae overlap region, although rare, is not a unique feature.

In addition, our improved model can serve as a solid

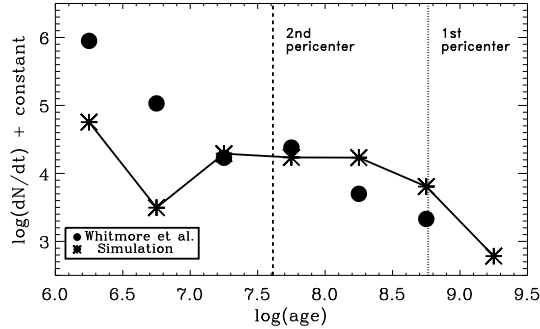


FIG. 4.— Formation rate of stellar particles versus age for our simulation (stars and solid line). Vertical lines indicate the time of first (dotted) and second (dashed) pericenter. The observed cluster formation rate from Whitmore et al. (2007) is given as filled circles.

basis and testbed for further theoretical studies of the enigmatic interacting NGC 4038/39 system. For example, the overlap region in the Antennae is dominated by molecular gas, which we do not model in the simulation presented here. Given that we now have a dynamically viable method for forming the overlap region, detailed investigations of the molecular gas formation process can be undertaken using improved theoretical models (e.g. Robertson & Kravtsov 2008; Pelupessy & Papadopoulos

2009). In a first application using this new orbital configuration we have been able to qualitatively and quantitatively reproduce the magnetic field morphology of the Antennae galaxies (Kotarba et al. 2009).

Finally, accurate modeling of nearby interacting systems also provide unique insights into the merger dynamics and timing of observed merger systems. The Antennae galaxies are traditionally in the first place in the classical Toomre sequence which orders galaxies according to their apparent merger stage (Toomre 1977) with the Mice (NGC 4676) being between their first and second pericenter (Barnes 2004) and thus in second place behind the Antennae. According to our proposed model the Antennae galaxies are in a later merger phase, after the second pericenter. As a consequence the Antennae would lose their first place, and thus requiring a revision of the classical Toomre sequence.

This work was supported by the DFG priority program 1177 and the DFG Cluster of Excellence “Origin and Structure of the Universe”. We would like to thank J. Hibbard, N. Bastian, B. Whitmore and M. Fall for valuable discussions on the manuscript. F. Renaud is a member of the IK I033-N Cosmic Matter Circuit at the University of Vienna.

#### REFERENCES

- Barnes, J. E. 1988, *ApJ*, 331, 699  
—, 1992, *ApJ*, 393, 484  
—, 2004, *MNRAS*, 350, 798  
Barnes, J. E. & Hernquist, L. 1996, *ApJ*, 471, 115  
Barnes, J. E. & Hibbard, J. E. 2009, *AJ*, 137, 3071  
Bastian, N., Trancho, G., Konstantopoulos, I. S., & Miller, B. W. 2009, *ApJ*, 701, 607  
Brandl, B. R., et al., 2009, *ApJ*, 699, 1982  
Bridge, C. R., Carlberg, R. G., & Sullivan, M. 2010, *ApJ*, 709, 1067  
Conselice, C. J., Bershady, M. A., Dickinson, M., & Papovich, C. 2003, *AJ*, 126, 1183  
Cox, T. J., Jonsson, P., Somerville, R. S., Primack, J. R., & Dekel, A. 2008, *MNRAS*, 384, 386  
Fall, S. M., Chandar, R., & Whitmore, B. C. 2005, *ApJ*, 631, L133  
Gao, Y., Lo, K. Y., Lee, S.-W., & Lee, T.-H. 2001, *ApJ*, 548, 172  
Hernquist, L. 1990, *ApJ*, 356, 359  
Hibbard, J. E., et al., 2005, *ApJ*, 619, L87  
Hibbard, J. E., van der Hulst, J. M., Barnes, J. E., & Rich, R. M. 2001, *AJ*, 122, 2969  
Hopkins, P. F., Hernquist, L., Cox, T. J., Di Matteo, T., Martini, P., Robertson, B., & Springel, V. 2005, *ApJ*, 630, 705  
Johansson, P. H., Naab, T., & Burkert, A. 2009, *ApJ*, 690, 802  
Karl, S. J., Naab, T., Johansson, P. H., Theis, C., & Boily, C. M. 2008, *Astronomische Nachrichten*, 329, 1042  
Kotarba, H., Karl, S. J., Naab, T., Johansson, P. H., Dolag, K., Lesch, H., & Stasyszyn, F. A. 2009, *ArXiv e-prints*, arXiv:0911.3327  
Lotz, J. M., et al., 2008, *ApJ*, 672, 177  
Mihos, J. C., Bothun, G. D., & Richstone, D. O. 1993, *ApJ*, 418, 82  
Mihos, J. C. & Hernquist, L. 1996, *ApJ*, 464, 641  
Mirabel, I. F., et al., 1998, *A&A*, 333, L1  
Mo, H. J., Mao, S., & White, S. D. M. 1998, *MNRAS*, 295, 319  
Naab, T. & Burkert, A. 2003, *ApJ*, 597, 893  
Naab, T., Jesseit, R., & Burkert, A. 2006, *MNRAS*, 372, 839  
Naab, T. & Ostriker, J. P. 2009, *ApJ*, 690, 1452  
Neff, S. G. & Ulvestad, J. S. 2000, *AJ*, 120, 670  
Patton, D. R., et al., 2002, *ApJ*, 565, 208  
Pelupessy, F. I. & Papadopoulos, P. P. 2009, *ApJ*, 707, 954  
Renaud, F., Boily, C. M., Fleck, J., Naab, T., & Theis, C. 2008, *MNRAS*, 391, L98  
Renaud, F., Boily, C. M., Naab, T., & Theis, C. 2009, *ApJ*, 706, 67  
Robertson, B. E. & Kravtsov, A. V. 2008, *ApJ*, 680, 1083  
Rothberg, B. & Joseph, R. D. 2004, *AJ*, 128, 2098  
Saviane, I., Momany, Y., da Costa, G. S., Rich, R. M., & Hibbard, J. E. 2008, *ApJ*, 678, 179  
Schweizer, F., et al., 2008, *AJ*, 136, 1482  
Springel, V. 2000, *MNRAS*, 312, 859  
—, 2005, *MNRAS*, 364, 1105  
Springel, V., Di Matteo, T., & Hernquist, L. 2005, *MNRAS*, 361, 776  
Springel, V. & Hernquist, L. 2003, *MNRAS*, 339, 289  
Tacconi, L. J., et al., 2010, *Nature*, 463, 781  
Tacconi, L. J., Genzel, R., Tecza, M., Gallimore, J. F., Downes, D., & Scoville, N. Z. 1999, *ApJ*, 524, 732  
Toomre, A. 1977, in *Evolution of Galaxies and Stellar Populations*, ed. B. M. Tinsley & R. B. Larson, 401–+  
Toomre, A. & Toomre, J. 1972, *ApJ*, 178, 623  
Wang, Z., et al., 2004, *ApJS*, 154, 193  
Whitmore, B. C., Chandar, R., & Fall, S. M. 2007, *AJ*, 133, 1067  
Whitmore, B. C., Zhang, Q., Leitherer, C., Fall, S. M., Schweizer, F., & Miller, B. W. 1999, *AJ*, 118, 1551  
Xu, C., Gao, Y., Mazzarella, J., Lu, N., Sulentic, J. W., & Domingue, D. L. 2000, *ApJ*, 541, 644  
Zezas, A., Fabbiano, G., Baldi, A., Schweizer, F., King, A. R., Ponman, T. J., & Rots, A. H. 2006, *ApJS*, 166, 211  
Zhang, Q., Fall, S. M., & Whitmore, B. C. 2001, *ApJ*, 561, 727